Copper-manganese oxide catalysts prepared by solution combustion synthesis for total oxidation of VOCs

(Article begins on next page)

01 August 2024

# Copper-manganese oxide catalysts prepared by solution combustion synthesis for total oxidation of VOCs

Clarissa Cocuzza, Enrico Sartoretti, Chiara Novara, Fabrizio Giorgis, Samir Bensaid, Nunzio Russo, Debora Fino, Marco Piumetti [*]

*Department of Applied Science and Technology, Politecnico di Torino, Corso Duca degli Abruzzi, 24, 10129 Turin, Italy*

A B S T R A C T

A set of Cu-Mn oxides was prepared through the simple and effective solution combustion synthesis method by varying the relative amount of copper and manganese. The physico-chemical properties of the samples were investigated through complementary techniques such as $N_2$ physisorption at $-196$ °C, XRD, HR-TEM, Raman spectroscopy, temperature programmed analyses ($H_2$-TPR, $O_2$-TPD, and $NH_3$-TPD), and XPS. The prepared catalysts were tested for the total oxidation of volatile organic compounds (ethylene, propylene, and toluene). The best performances, in terms of total VOC oxidation, were achieved with a copper content ranging from 15 at % to 45 at%. The catalytic test outcomes demonstrate the beneficial effect of acidic sites, oxygen mobility, and redox ability. In particular, ethylene oxidation is mainly favored by oxygen vacancies and redox properties, while propylene and toluene oxidation is mostly enhanced by acidic sites. All the catalysts prepared can totally oxidize the examined pollutants examined below 310 °C. Moreover, the binary oxides exhibit good catalytic stability over a time-on-stream of 7 h and low water vapor inhibition (5 vol% $H_2O$ in the gas stream).

## 1. Introduction

Volatile organic compounds (VOCs) are organic molecules of low molecular weight. They are pollutants emitted from variable sources, for instance, transport, industrial processes, and household chores [1]. Exposure to VOCs is a hazard for humans because they are carcinogenic, teratogenic, toxic, and mutagenic [2]. Moreover, VOCs also negatively affect the environment because they are considered one of the main factors responsible for photochemical smog, the formation of tropospheric ozone, and stratospheric ozone depletion [3]. The most suitable technique for the abatement of these organic molecules is oxidizing them to carbon dioxide and water. Among the procedures based on oxidation, the conventional strategy is thermal incineration. However, it is an expensive operation due to the elevated temperature necessary for the complete oxidation of VOCs, typically 800–1200 °C, and additional fuel is required to achieve these temperatures. To achieve efficient abatement, VOCs must be completely oxidized, because partial or poorly controlled thermal oxidation can produce toxic byproducts such as dioxins and carbon monoxide [4]. Catalytic oxidation is a more thermally effective and environmentally friendly technique because it requires lower temperatures to achieve the complete destruction of VOCs; in

addition, catalytic oxidation limits the formation of dioxins and harmful byproducts, such as NOx, which are produced during thermal incineration at high temperatures [1,5].

Previous research has established that noble metals are the most active catalysts that can be employed for the catalytic oxidation of VOCs. In fact, they completely oxidize these pollutants at very low temperature [6]. In fact, studies such as conducted by Liotta (2010) have shown that in presence of Pt the complete oxidation of propene is achieved at 170 °C and the complete oxidation of toluene at 250 °C [7]. Despite their high activity, they are very expensive and subject to deactivation by sintering or poisoning. Transition metal oxides have recently been considered a promising alternative to noble metals because, despite their lower activity, they are less expensive and more resistant to deactivation [8,9].

The main aim of this study is to investigate the catalytic oxidation efficiency of manganese and copper mixed oxides. In this work, a series of Cu-Mn oxide catalysts (with different Mn/Cu atomic ratios) were synthesized and compared with the pure oxides $Mn_2O_3$ and CuO. As it has previously been observed the binary systems should have more elevated oxygen mobility than the pure oxides of Mn and Cu, and consequently a higher activity [10]. Manganese oxides are promising catalysts due to their low cost and high efficiency in the oxidation of

* Corresponding author.
 *E-mail address:* marco.piumetti@polito.it (M. Piumetti).

**Table 1**

Textural and structural properties of samples, derived from $N_2$ physisorption at − 196 °C, XRD, and EDS analyses.

| Catalyst | $S_{BET}^a$ $(m^2/g)$ | $V_P^b$ $(cm^3/g)$ | Mn at %[c] | Cu at %[c] | Phase | Crystallite-size $(nm)^d$ |
|---|---|---|---|---|---|---|
| $Mn_2O_3$ | 21.9 | 0.15 | - | - | $Mn_2O_3$ | 57 |
| $Mn_{85}Cu_{15}$ | 14.7 | 0.14 | 86 | 14 | $Mn_2O_3$ | 100 |
| | | | | | $CuMn_2O_4$* | 65 |
| $Mn_{70}Cu_{30}$ | 11.0 | 0.07 | 69 | 31 | $CuMn_2O_4$ | 75 |
| | | | | | $Mn_2O_3$ | 96 |
| $Mn_{55}Cu_{45}$ | 8.4 | 0.04 | 54 | 46 | $CuMn_2O_4$ | 71 |
| $Mn_{40}Cu_{60}$ | 8.0 | 0.04 | 43 | 57 | $CuMn_2O_4$ | 59 |
| | | | | | CuO | 44 |
| $Mn_{25}Cu_{75}$ | 5.5 | 0.03 | 22 | 78 | CuO | 43 |
| | | | | | $CuMn_2O_4$ | 63 |
| CuO | 2.6 | 0.01 | - | - | CuO | 65 |

a → Specific surface area calculated by applying BET method.

b → Total pore volume according to the BJH method, approximating the pores to cylindrical ones.

c → Atomic concentration relative to the metals present in the oxides, derived from EDS analysis on at least two different areas.

d → Crystallite size calculated through the Scherrer formula.

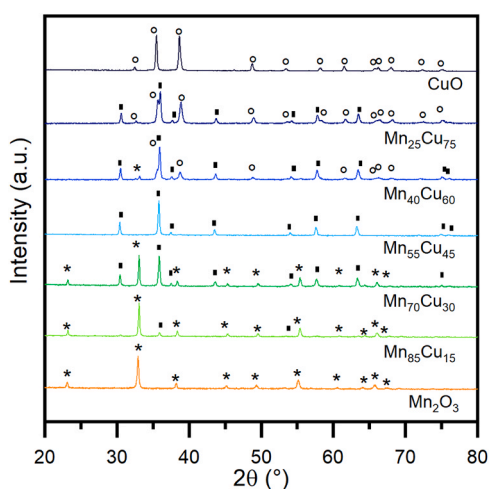* → The crystallite size was calculated on the two main peaks.



**Fig. 1.** Powder XRD patterns of the synthesized catalysts. * → $Mn_2O_3$ ref. 00-041, ▪ → $CuMn_2O_4$ ref. 01-074, O → CuO ref. 01-089.

**Table 2**

Relative amounts of crystalline phases, XRD peak intensity ratio, and semi-quantitative amounts of 110 face.

| Catalyst | Crystalline phase (%) | | XRD intensity ratio | | (110) face (%) |
|---|---|---|---|---|---|
| | $Mn_2O_3$ | $CuMn_2O_4$ | $\frac{(440)_{Mn_2O_3}}{(222)}$ | $\frac{(220)_{CuMn_2O_4}}{(311)}$ | |
| $Mn_2O_3$ | 100 | - | 0.28 | - | 28 |
| $Mn_{85}Cu_{15}$ | 81 | 19 | 0.26 | 0.26 | 26 |
| $Mn_{70}Cu_{30}$ | 30 | 70 | 0.29 | 0.36 | 34 |
| $Mn_{55}Cu_{45}$ | - | 100 | - | 0.37 | 37 |
| $Mn_{40}Cu_{60}$ | 3 | 69 | - | 0.35 | 24 |
| $Mn_{25}Cu_{75}$ | - | 42 | - | 0.32 | 13 |
| CuO | - | - | - | - | 0 |

oxide phases interacting with each other, because this phenomenon will induce the formation of oxygen vacancies [2]. Among the possible transition metals, copper was chosen to realize mixed oxides because Mn-Cu oxides are reported to be active for VOC abatements [13].

Among the possible synthesis techniques, the solution combustion synthesis (SCS) method was adopted to prepare the Cu-Mn oxides studied in this research. This procedure is based on a highly exothermic redox reaction occurring in the solution of precursors. The SCS technique is very interesting because it is easy to implement and allows to obtain nanostructured oxides with the desired composition [14]. The starting solution contains metal precursors and an organic fuel compound that improves the properties of the oxides, such as higher surface area and better oxygen mobility [15].

The synthesized Cu-Mn oxides were tested for the catalytic oxidation of ethylene, propylene, and toluene, chosen as representative molecules of a wide range of VOCs. The most active catalysts were also tested in the presence of water vapor to simulate real conditions. This study was set out to evaluate how effective are the prepared Cu-Mn oxides prepared for the catalytic oxidation of VOCs, in the perspective of using them in stationary implants.

## 2. Experimental

### 2.1. Catalyst preparation

A series of Cu-Mn oxide catalysts with different Mn/Cu atomic ratios (hereafter referred to as $Mn_xCu_{100-x}$, where x means Mn/(Mn+Cu)* 100) were prepared via the SCS method as previously mentioned. Suitable amounts of the metal precursors $Mn(NO_3)_2 \bullet 4 H_2O$ (Sigma—Aldrich) and $Cu(NO_3)_2 \bullet 3 H_2O$ (Emsure) were dissolved in 50 mL of deionized water to obtain a solution of 0.2 M. Citric acid monohydrate (Sigma—Aldrich) was added to the solution at the same concentrations as the metal precursors. The solution was then energetically stirred at room temperature for 10 min. Subsequently, the solution was heated to 650 °C in an oven (heating ramp 5 °C $min^{-1}$) and kept at this temperature for 30 min

### 2.2. Catalyst characterization

The physico-chemical properties of the synthesized samples were investigated by complementary techniques. $N_2$ physisorption analysis was performed at − 196 °C (Micromeritics Tristar II 3020) on oxide powders previously outgassed at 200 °C for 2 h to remove the substances absorbed on surfaces, such as moisture and other atmospheric pollutants. Through $N_2$ physisorption analysis, the specific surface area ($S_{BET}$) and total pore volume ($V_P$) were determined, and the former was calculated according to the Brunauer, Emmet, and Teller method.

The X-ray diffraction (XRD) patterns, obtained on an X′ Pert Philips PW3040 diffractometer adopting Cu Kα radiation (range of 2θ: 20–80°, step: 0.05° 2θ, time per step: 0.2 s), were examined using the Powder Data File Databases (PDF-2 Release 2004, COD_Mar10). Scherrer's formula was used to estimate the average crystallite sizes of the Cu-Mn oxides using a shape factor of 0.9.

The morphology of the samples was studied through transmission electron microscopy (TEM, Jeol JEM 3010 UHR, LaB₆ gun, operating at 200 kV). EDS analyses (Oxford X-stream) were performed to determine the chemical compositions of the prepared catalysts.

Raman spectra were acquired at room temperature using a Renishaw InVia Reflex micro-Raman spectrometer. The excitation was provided by a solid-state laser emitting at 514.5 nm, whose power was set to 1 mW to avoid overheating of the sample during the measurement. Three spectra were collected in different regions of each material to verify its homogeneity using a 20x objective and a total acquisition time of 225 s

The reducibility and the oxygen desorption analyses were performed in the ThermoQuest TPD/R/O 1100 instrument using the thermal conductivity detector with which it is provided. The reducibility of the

VOCs, thanks to the coexistence of various valence states that allow the presence of ionic couples ($Mn^{(n+1)+}/Mn^{n+}$) on the surface that facilitate redox cycles [11]. Moreover, the catalytic activity can be improved by doping $MnO_x$ with transition metals, which increases the presence of defect sites, enhancing reducibility and oxygen mobility [12]. The catalytic properties can also be enhanced by the copresence of different
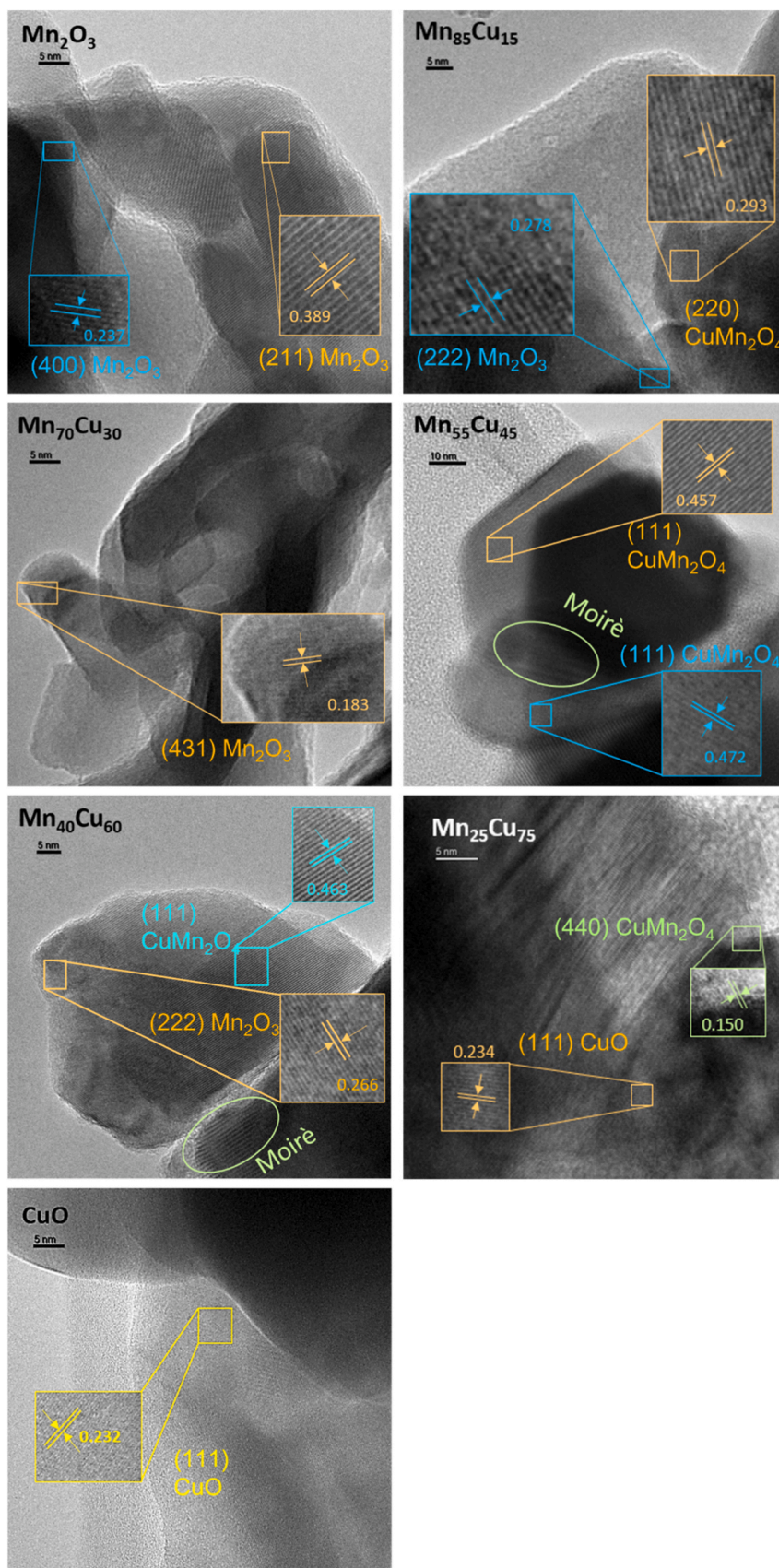
**Fig. 2.** HR-TEM images highlighting the fringes identified on the samples.
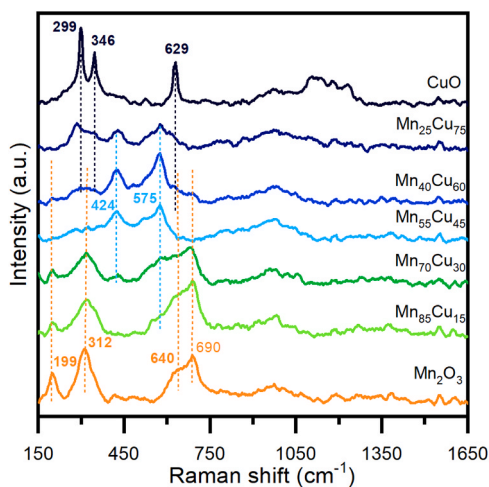
**Fig. 3.** Raman spectra of the synthesized samples collected at room temperature.
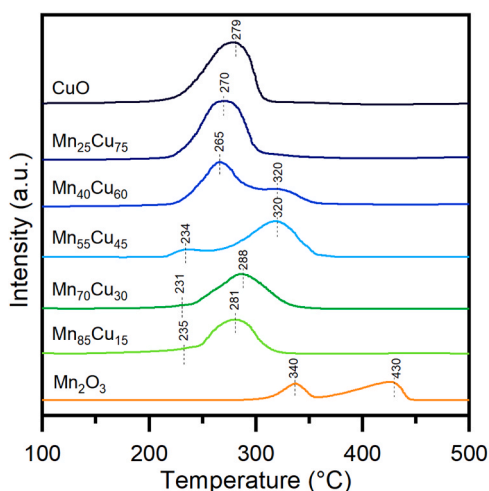


**Fig. 4.** $H_2$-TPR profiles of the synthesized samples.

**Table 3**
$H_2$-uptake (mmol $g_{cat}^{-1}$) obtained by $H_2$-TPR analysis, and $O_2$ desorbed (μmol $g_{cat}^{-1}$) acquired by $O_2$-TPD analysis.

| Catalyst | Total $H_2$ consumption | $H_2$-uptake 200–299 °C | $H_2$-uptake 300–399 °C | $H_2$-uptake T > 400 °C | Total $O_2$ desorbed |
|---|---|---|---|---|---|
| $Mn_2O_3$ | 7.12 | - | 2.13[a] | 4.98[b] | 6.55 |
| $Mn_{85}Cu_{15}$ | 8.70 | 8.70[c] | - | - | 2.82 |
| $Mn_{70}Cu_{30}$ | 10.41 | 10.41[c] | - | - | 6.57 |
| $Mn_{55}Cu_{45}$ | 11.32 | 1.34[d] | 9.98[c] | - | 9.11 |
| $Mn_{40}Cu_{60}$ | 11.92 | 7.46[d] | 4.46[c] | - | 6.79 |
| $Mn_{25}Cu_{75}$ | 13.20 | 13.20[d] | - | - | 1.45 |
| CuO | 14.70 | 14.70[d] | - | - | 0.93 |

a: $Mn_2O_3 \rightarrow Mn_3O_4$.
b: $Mn_3O_4 \rightarrow MnO$.
c: $Mn_2O_3 \rightarrow MnO$.
d: $CuO \rightarrow Cu^0$.

catalysts was investigated by subjecting the samples to a flow of hydrogen, simultaneously increasing the temperature in a controlled way. Before the $H_2$-TPR analysis, the sample powder must undergo a pre-treatment: 30 mg of sample powder was placed in a tubular quartz reactor and treated with helium (30 mL $min^{-1}$) at 550 °C for 60 min (heating ramp equal to 10 °C $min^{-1}$), then it was cooled down fluxing
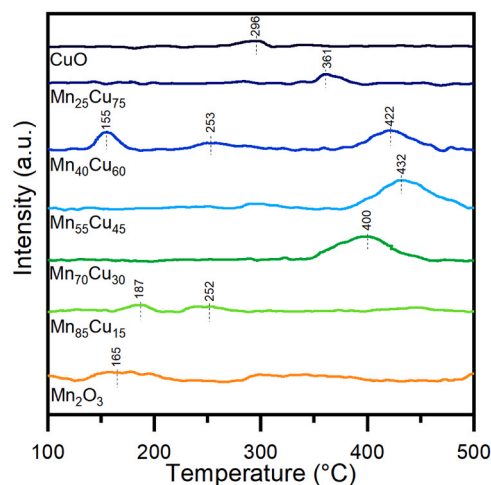


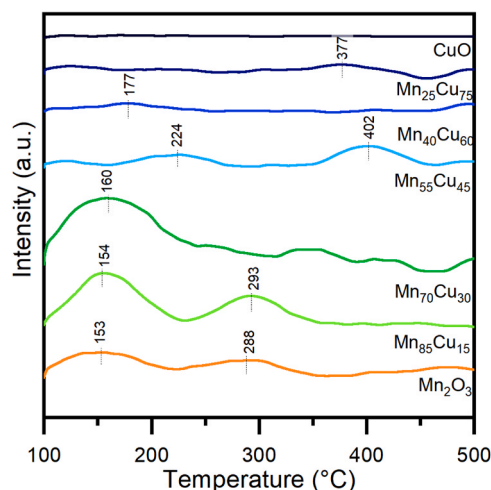**Fig. 5.** $O_2$-TPD profiles of the synthesized samples.



**Fig. 6.** $NH_3$-TPD profiles of the synthesized samples.

**Table 4**
$NH_3$ desorbed (μmol $g_{cat}^{-1}$) obtained by $NH_3$-TPD analysis.

| Catalyst | Total $NH_3$ desorption | $NH_3$-desorbed 100–250 °C | $NH_3$-desorbed 250–410 °C |
|---|---|---|---|
| $Mn_2O_3$ | 0.09 | 0.06 | 3.6 $10^{-2}$ |
| $Mn_{85}Cu_{15}$ | 0.17 | 0.12 | 5.2 $10^{-2}$ |
| $Mn_{70}Cu_{30}$ | 0.15 | 0.15 | 0.0 |
| $Mn_{55}Cu_{45}$ | 0.07 | 0.02 | 4.5 $10^{-2}$ |
| $Mn_{40}Cu_{60}$ | 0.02 | 0.01 | 0.9 $10^{-2}$ |
| $Mn_{25}Cu_{75}$ | 0.01 | 0.0 | 0.9 $10^{-2}$ |
| CuO | 0.0 | 0.0 | 0.0 |

He. The analysis was conducted with programmed heating (from 50 °C to 700 °C, heating ramp 5 °C $min^{-1}$, the final temperature was held for 10 min) exposing the powder to a reducing gas flow (5 vol% of $H_2$ in Ar, 20 mL $min^{-1}$). To analyze the oxygen desorption, 250 mg of Cu-Mn oxide powder was first pre-treated with a flow of pure oxygen (20 mL $min^{-1}$) at 600 °C for 60 min; the samples were then cooled down in $O_2$. The test was performed by flowing He (10 mL $min^{-1}$) and heating the sample to 550 °C (heating ramp equal to 5 °C $min^{-1}$).

The ammonia desorption analyses were performed in the ALTAMIRA AMI300 Lite TPD/R/O instrument, the signal was acquired using a thermal conductivity detector, and the sample temperature was monitored with a thermocouple placed near the catalytic bed. The sample
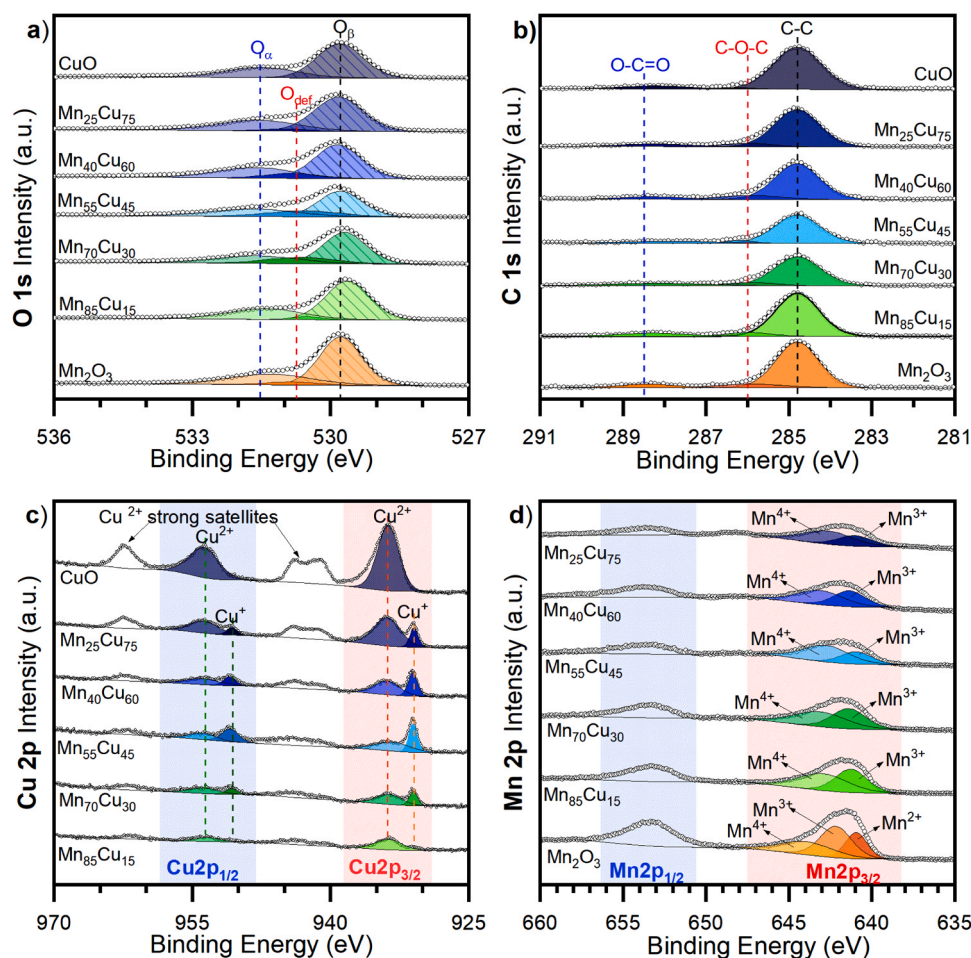
**Fig. 7.** XPS spectra of the synthesized samples in the a) O 1 s b) Mn 2p c) Cu 2p core level regions.

**Table 5**
Redox couple ratios, $Mn^{4+}$ and $Cu^+$ relative abundance, and oxygen ratios derived from deconvoluted XPS spectra.

| Catalyst | $O_\alpha/O_\beta$ | $O_{def}$ (%) | $Mn^{3+}/Mn^{2+}$ | $Mn^{4+}/Mn^{3+}$ | $Mn^{4+}$ (%) | $Cu^{2+}/Cu^+$ | $Cu^+$ (%) |
|---|---|---|---|---|---|---|---|
| $Mn_2O_3$ | 0.05 | 7.4 | 1.74 | 0.71 | 31.0 | - | - |
| $Mn_{85}Cu_{15}$ | 0.47 | 3.6 | - | 1.14 | 53.4 | - | - |
| $Mn_{70}Cu_{30}$ | 0.46 | 18.1 | - | 1.15 | 53.4 | 2.69 | 27.1 |
| $Mn_{55}Cu_{45}$ | 0.58 | 19.8 | - | 1.97 | 66.4 | 1.25 | 44.3 |
| $Mn_{40}Cu_{60}$ | 0.53 | 10.1 | - | 1.31 | 56.8 | 1.72 | 36.8 |
| $Mn_{25}Cu_{75}$ | 0.52 | 4.1 | - | 1.84 | 64.7 | 4.54 | 18.0 |
| CuO | 0.48 | 0 | - | - | - | - | - |

(50 mg) was inserted into a quartz U-tube reactor in a fixed-bed configuration. The sample was pretreated with helium (25 mL min$^{-1}$) at 600 °C for 30 min (heating ramp equal to 10 °C min$^{-1}$) and then cooled to 100 °C. A flow of 2500 ppm NH$_3$ in He (35 mL min$^{-1}$) was kept for 2 h at 100 °C, and finally, helium (35 mL min$^{-1}$) was flowed for 30 min. The NH$_3$-TPD analysis was performed by flowing 20 mL min$^{-1}$ He in the temperature range of 100–500 °C.

XPS (X-ray photoelectron spectroscopy) spectra were acquired using the XPS PHI 5000 Versa probe apparatus. The conditions adopted were a bandpass energy of 187.85 eV, a 45° take-off angle, and a 100.0 μm diameter X-ray spot size.

*2.3. Catalytic activity test*

To evaluate the catalytic performance of VOC oxidation, 0.1 g of

oxide powder in pellet form (size of 212–300 μm) was introduced into a quartz U-tube reactor (ID=4 mm) in a fixed-bed configuration. The reactor was heated by an electric furnace, and the temperature of the catalytic bed was measured using a thermocouple placed in its proximity. Before the test, the sample was pre-treated at 150 °C for 60 min flowing N$_2$ with the same flow rate adopted for the test.

The test was started at 70 °C, and once chemical equilibrium was reached, the temperature was increased by 30 °C until complete oxidation of the pollutant. The gas reactive mixture flowing in the reactor contains 10 vol% O$_2$, a VOC at different concentrations as a function of the tested molecule (500 ppm ethylene, 500 ppm propylene, and 250 ppm toluene) and N$_2$ to balance. During the test, the parameter W/F= 0.044 g h L$^{-1}$ corresponding approximately to a GHSV of 20,000 h$^{-1}$ was maintained.

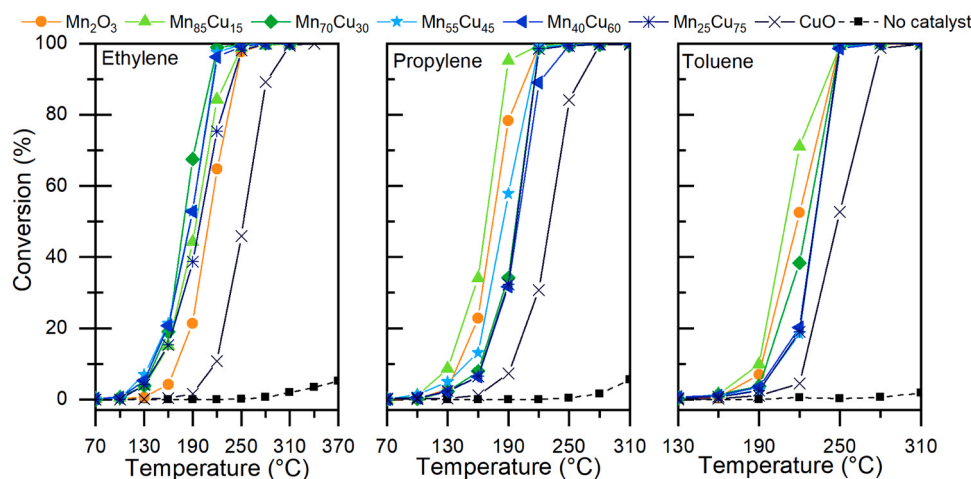The VOCs conversion was estimated by the reactor outlet concen-

**Fig. 8.** Catalytic oxidation of ethylene (500 ppm), propylene (500 ppm), and toluene (250 ppm) over the mixed oxides prepared. Gas feed conditions: W/F= 0.044 g h L$^{-1}$, 10 vol% O$_2$, and N$_2$ to balance.

**Table 6**
Results from catalytic oxidation of ethylene, propylene, and toluene tests.

| Catalyst | Ethylene rate$^a$ ($\mu mol\ h^{-1}\ m^{-2}$) | Propylene rate$^a$ ($\mu mol\ h^{-1}\ m^{-2}$) | Toluene rate$^b$ ($\mu mol\ h^{-1}\ m^{-2}$) |
|---|---|---|---|
| Mn$_2$O$_3$ | 0.3 | 0.7 | 0.8 |
| Mn$_{85}$Cu$_{15}$ | 1.6 | 5.4 | 1.6 |
| Mn$_{70}$Cu$_{30}$ | 2.3 | 1.0 | 0.9 |
| Mn$_{55}$Cu$_{45}$ | 5.9 | 3.2 | 0.8 |
| Mn$_{40}$Cu$_{60}$ | 3.7 | 1.4 | 1.1 |
| Mn$_{25}$Cu$_{75}$ | 5.4 | 2.3 | 1.1 |
| CuO | 0.8 | 0.6 | 0.9 |

a → Rates evaluated at 130 °C.
b → Rates evaluated at 190 °C.

tration of CO$_2$ and CO, measured by a non-dispersive infrared (NDIR) analyzer (ABB Uras 14), using Eq. (1):

$$conv_{VOC} = \left[1 - \left(\frac{c_{VOC} - \frac{c_{CO_2}}{x} - \frac{c_{CO}}{x}}{c_{VOC}}\right)\right] \times 100 \qquad (1)$$

where conv$_{VOC}$ is the achieved conversion of the VOC present in the input flow (%), c$_{VOC}$ is the inlet VOC concentration (ppm), c$_{CO_2}$ and c$_{CO}$ are the outlet CO$_2$ and CO concentrations respectively (ppm), and x is the number of carbon atoms in the VOC molecule, C$_x$H$_y$.

The specific oxidation rates at a temperature T (rate$_T$) can be calculated adopting Eq. (2) and Eq. (3):

$$\dot{n}_{VOC,T} = conv_{VOC,T} \times \dot{n}_{TOT} \qquad (2)$$

$$rate_T = \frac{\dot{n}_{VOC,T}}{m_{cat} \times S_{BET}} \qquad (3)$$

where, n$_{VOC,T}$ is the oxidized VOC molar flow at temperature T (mol h$^{-1}$), n$_{TOT}$ is the total inlet molar flow of VOC (mol h$^{-1}$), conv$_{VOC,T}$ is the VOC conversion at temperature T (%), as expressed in Eq. (1), m$_{cat}$ is the amount of catalyst present in the reactor (0.1 g), SBET is the specific surface area of the catalyst estimated from N$_2$ physisorption at − 196 °C (m$^2$ g$^{-1}$) and rate$_T$ is the VOC specific oxidation rate at temperature T (mol h$^{-1}$ m$^{-2}$).

To measure the stability of the catalytic performance, additional tests were conducted on the best performing Cu-Mn oxide for each VOC considered. To evaluate the stability of the catalysts, oxidation of the pollutant molecule for three consecutive runs, and time-on-stream tests at alternating temperatures and at a fixed temperature, oxidation in wet conditions (water vapor 5 vol%) were carried out.
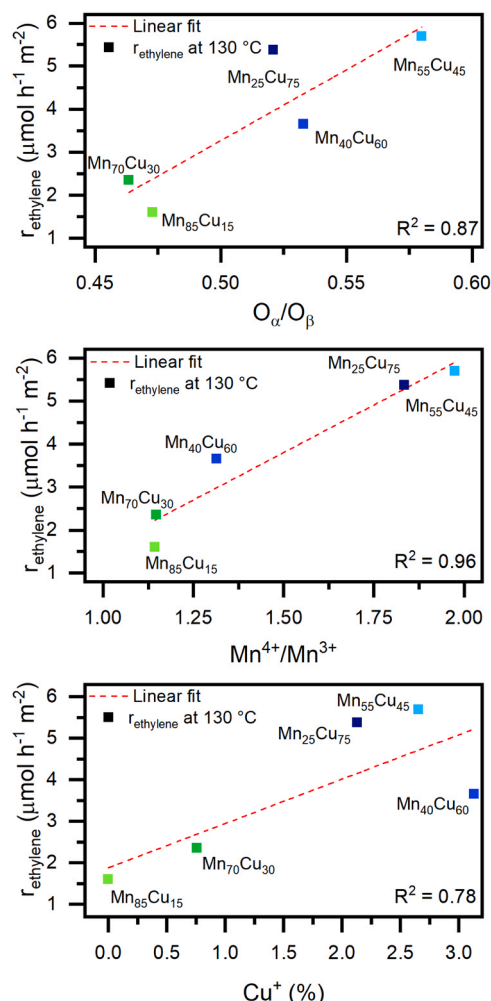


**Fig. 9.** Correlation between O$_\alpha$/O$_\beta$ ratio, Mn$^{4+}$/Mn$^{3+}$ ratio, and Cu$^+$ (%) and ethylene oxidation rate for the binary oxides.
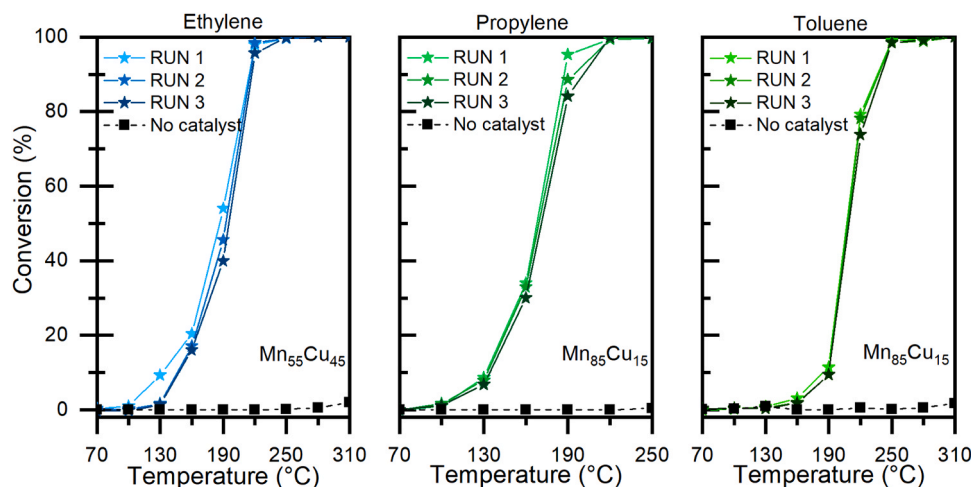
**Fig. 10.** Stability study of $Mn_{55}Cu_{45}$ for the catalytic oxidation of ethylene (500 ppm) and $Mn_{85}Cu_{15}$ for the catalytic oxidation of propylene (500 ppm) and toluene (250 ppm), for three successive oxidation runs. Gas feed conditions: $W/F = 0.044$ g h $L^{-1}$, 10 vol% $O_2$, and $N_2$ to balance.

## 3. Results and discussion

### 3.1. Characterization of samples

Table 1 reports the main textural properties of the oxides studied in this work, obtained with $N_2$ physisorption, XRD, and EDS analyses.

As a whole, the prepared samples have similar values of specific surface area and total pore volume, which enables a reliable comparison of the catalysts prepared in the catalytic tests [1].

The peaks of the XRD diffraction patterns are shown in Fig. 1, and they can be related to manganese oxide (III) (ref. 00-041), copper oxide (II) (ref. 01-089), and spinel $CuMn_2O_4$ (ref. 01-074).

The narrow and sharp peaks show a high level of crystallization [16]. Increasing the copper content progressively increases the intensity of the diffraction peaks ascribed to the $CuMn_2O_4$ phase; in particular, the peak located at 35.85° corresponds to the (311) lattice plane, the most intense reflection peak of the spinel [17]. For sample $Mn_{55}Cu_{45}$, the only phase present is spinel $CuMn_2O_4$. Upon increasing the copper content, diffraction peaks related to the CuO phase appear with increasing intensity. The $Mn_{40}Cu_{60}$ sample presents a peak of low intensity at 32.95° that could be due to the (222) lattice plane of $Mn_2O_3$, the most intense reflection peak for manganese oxide [18]. Most likely, due to the formation of CuO, manganese is in excess to form solely $CuMn_2O_4$, and a small amount of the $Mn_2O_3$ phase appears. On the other hand, for the $Mn_{55}Cu_{45}$ sample, despite the Cu content being superior to that necessary for obtaining $CuMn_2O_4$, there is no presence of diffraction peaks corresponding to the CuO phase. It is possible that CuO nanocrystallites are very well dispersed and for this reason not detectable by the diffractometer or the Cu in excess can be present in the amorphous form (vide infra).

The relative amount of each crystalline phase was calculated by the HighScore Plus software. The values are reported in Table 2. It is important noticing that $Mn_2O_3$ and $CuMn_2O_4$ present {110} crystal planes, in particular $Mn_2O_3$ presents (440) crystal planes and $CuMn_2O_4$ presents (220) and (440) crystal planes. As previously reported, by Dosa et al. by evaluating the ratio between the intensity of the most representative peak related to 110 and the intensity of the highest peak for each phase it is possible to estimate the relative abundance of {110} crystal faces [19]. By multiplying the relative of the crystalline phases by the ratio of the peaks' intensity, it is possible to obtain a semi-quantitative amount of 110 crystal faces present in each sample. The {110} crystal planes provide a high catalytic activity for VOC oxidation due to the high amount of oxygen vacancies [20].

The general appearance of the Cu-Mn oxides is shown in HR-TEM

images in Fig. S1. Sample aggregates present a heterogeneous morphology with bubble-shaped concavities, probably due to the gases released during the synthesis process [21]. The images of the prepared catalysts display elongated structures rich in manganese and pebble-like structures rich in copper. The $Mn_{55}Cu_{45}$ sample exhibits polyhedral structures (Mn 69 at% and Cu 31 at%) that can be reconducted to the spinel $CuMn_2O_4$. According to Fig. S1, the oxides with higher amount of manganese ($Mn_2O_3$, $Mn_{85}Cu_{15}$, and $Mn_{70}Cu_{30}$) seem to have a more accessible 3-D structure.

Fig. 2 shows the HR-TEM images of the synthesized samples obtained at higher magnification. Except for $Mn_2O_3$, $Mn_{55}Cu_{45}$, and CuO, the catalysts have a polyphasic structure, in agreement with the XRD patterns. As a result of different crystalline planes overlapping, Moirè - fringes can be detected on different samples [22]. In addition, amorphous domains can be recognized on the edges of the particles; the missing amount of Cu in $Mn_{55}Cu_{45}$, according to the XRD pattern, may be present in these amorphous areas.

Raman spectroscopy was performed on all the synthesized samples, and the resulting spectra are shown in Fig. 3. The acquisition parameters were optimized to avoid excessive localized heating that would cause a phase transition of manganese species [23]. Except for $Mn_2O_3$, $Mn_{55}Cu_{45}$, and CuO, which display only signals related to $Mn_2O_3$, $CuMn_2O_4$, and CuO, respectively, the samples studied are constituted by a combination of these three crystalline phases. In particular, the peaks at 199, 312, 640, and 690 $cm^{-1}$ can be assigned to $Mn_2O_3$ [24,25]; the signals at 299, 346, and 629 $cm^{-1}$ are characteristic of CuO [25,26]; and the peaks at 424 and 575 $cm^{-1}$ can be ascribed to $CuMn_2O_4$ [25]. Hence, the Raman spectroscopy results fully support and agree with the XRD outcomes and TEM analysis.

To investigate the reactivity of the oxygen species in the samples, $H_2$-TPR analysis was performed on Cu-Mn oxides and the pure oxides $Mn_2O_3$ and CuO. The reduction profiles obtained are reported in Fig. 4. The pure CuO profile presents a single reduction peak at approximately 279 °C, ascribed to $Cu^{2+} \rightarrow Cu^0$ according to the literature [2,27]. The $Mn_2O_3$ profile is characterized by two peaks at 340 °C and 430 °C: the former can be related to the reduction step $Mn_2O_3 \rightarrow Mn_3O_4$, while the second is correlated to the final reduction step $Mn_3O_4 \rightarrow MnO$ [1,2,28]. As demonstrated by XRD and Raman analyses, $Mn_{55}Cu_{45}$ is only composed of $CuMn_2O_4$ spinel: the two characteristic peaks at 234 °C and 320 °C in its reduction profile can therefore be associated with $Cu^{2+} \rightarrow Cu^0$ and $Mn_2O_3 \rightarrow MnO$, respectively [29]. $Mn_{85}Cu_{15}$ and $Mn_{70}Cu_{30}$ present the main reduction peaks at 281 °C and 288 °C and shoulders at 235 °C and 231 °C, respectively; the main peak can be ascribed to $Mn_2O_3 \rightarrow MnO$ phase reduction, while the shoulder can be related to the
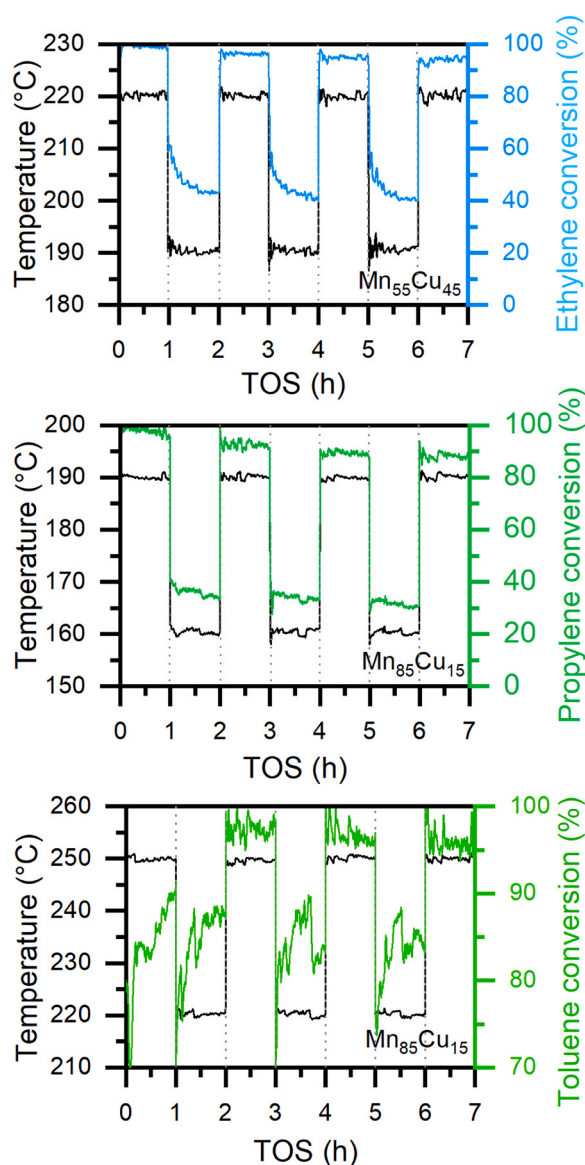
**Fig. 11.** Progression of ethylene (500 ppm), propylene (500 ppm), and toluene (250 ppm) conversion in the time-on-stream configuration under alternating temperatures. Gas feed conditions: W/F= 0.044 g h L$^{-1}$, 10 vol% O$_2$, and N$_2$ to balance.

reduction of the small amount of copper present (Cu$^{2+}$ → Cu$^0$). Mn$_{40}$Cu$_{60}$ exhibits a reduction profile very similar to CuMn$_2$O$_4$, with two peaks centered at 265 °C and 320 °C, but the higher intensity of the first peak suggests a larger amount of Cu$^{2+}$ species present with respect to Mn$_{55}$Cu$_{45}$, in line with XRD analysis. The profile reduction of Mn$_{25}$Cu$_{75}$ is characterized by a singular peak centered at 270 °C ascribed to Cu$^{2+}$ → Cu$^0$ reduction. The total H$_2$ consumption obtained for each sample is reported in Table 3. The H$_2$ uptake increases with increasing copper content. Cu-Mn oxides generally present lower reduction temperatures and consequently more reactive oxygen species than pure oxides. This fact is a confirmation of the positive effect of the copresence of multiple phases.

Fig. 5 shows the O$_2$-TPD profiles obtained for all the prepared samples. To obtain information related to the oxygen species of Cu-Mn oxides involved in the catalytic oxidation of VOCs, the analyses were carried out in the temperature range of 100 – 550 °C, which is the region characteristic of chemisorbed oxygen species (O$^-$, O$_2^-$) [1,30].

The Mn$_2$O$_3$ and Mn$_{85}$Cu$_{15}$ samples display only low-temperature

peaks of small intensity. The Mn$_{70}$Cu$_{30}$, Mn$_{55}$Cu$_{45}$, and Mn$_{25}$Cu$_{75}$ samples exhibit a peak at higher temperatures, while the Mn$_{40}$Cu$_{60}$ sample shows peaks at both low and high temperatures. In general, all the prepared catalysts release oxygen (even if in a small amount) in the temperature range analyzed; the estimated quantities of oxygen produced are reported in Table 3.

Since all samples desorb oxygen at a temperature below 450 °C, it can be supposed that a superficial mechanism occurs during VOC catalytic oxidation [30].

The temperature-programmed desorption of NH$_3$ was performed to study the acidic sites of the catalysts, and the profiles obtained are reported in Fig. 6. Mn$_{85}$Cu$_{15}$ and Mn$_{70}$Cu$_{30}$ display an evident peak at approximately 160 °C and a less intense peak at 294 °C and 347 °C, respectively. In contrast, the sample Mn$_{55}$Cu$_{45}$ shows the highest peak at 397 °C. The peaks at a lower temperature can be ascribed to weak Brønsted acidic sites. Above 200 °C, chemisorbed NH$_3$ desorption occurs, so the peaks at 294 °C, 347 °C, and 397 °C can be correlated to the stronger Lewis acidic sites [31,32]. The absence or very low intensity of desorption peaks in the other catalyst profiles revealed very weak or no acidic sites. Table 4 resumes the estimated quantities of ammonia desorbed.

XPS spectra in the C 1 s, O 1 s, Mn 2p, and Cu 2p core level regions are reported in Fig. 7, the redox couple and oxygen ratios are reported in Table 5, and the peak positions are listed in Table S1.

Fig. 7a shows the O 1 s spectra, in which three different peaks can be identified. The former in the 531.3 – 531.7 eV range is correlated to surface oxygen species O$_\alpha$ (OH$^-$, CO$_3$, O$_2^-$, O$^-$) [33,34]. The second peak in the 530.5 – 531.0 eV range may be ascribed to oxygen defects, particularly oxygen vacancies [35–37]. Finally, the third peak in the 529.6 – 529.8 eV range is attributed to lattice oxygen O$_\beta$ [14,38]. Except for the Mn$_2$O$_3$ and CuO samples, all the catalysts tested show Cu 2p (Fig. 7c) and Mn 2p (Fig. 7d) spectra characteristic of spinel CuMn$_2$O$_4$ [39]. The Cu 2p spectra of Cu-Mn oxides can be deconvoluted into two peaks attributed to Cu$^{2+}$ (930.9 – 931.1 eV) and Cu$^+$ (933.2 – 933.9 eV); the Cu$^{2+}$ peaks can be attributed to copper bound to lattice oxygen anions (O$^{2-}$) [38]. The Mn 2p spectra of Cu-Mn oxides present a peak that can be deconvoluted into two different peaks ascribed to Mn$^{4+}$ (642.6 – 644.0 eV) and Mn$^{3+}$ (641.0 – 642.2 eV), while the Mn$_2$O$_3$ sample displays an additional peak centered at 640.9 eV assigned to Mn$^{2+}$ [14]. As previously reported in the literature, a higher O$_\alpha$/O$_\beta$ ratio is usually connected to an increase in VOC oxidation activity [40]. Catalyst surfaces rich in O$_\alpha$ species can promote the oxygen spillover phenomenon due to enhanced electron mobility on the surface [19]. Moreover, it is well known that the amount of oxygen defects (O$_{def}$), particularly oxygen vacancies, is correlated with enhanced catalytic activity; in fact, O$_V$ of the oxides' lattice can bind to the molecular O$_2$ present in the gas phase, generating O$_2^{*-}$ that will more easily react with VOC molecules [41,42]. Other important parameters are the presence of redox couples, such as Mn$^{4+}$/Mn$^{3+}$ [40], and the presence of Cu$^+$ species [38] because they improve the catalyst oxidation efficiency.

### 3.2. Catalytic tests

The catalytic performances of the prepared Cu-Mn oxides toward the oxidation of ethylene, propylene, and toluene were studied in the 70–370 °C temperature range. The conversion curves obtained for the three VOCs are shown in Fig. 8.

For the abatement of ethylene, the catalytic performances achieved with Cu-Mn oxides are very similar and higher than that of pure oxides (Mn$_2$O$_3$ and CuO); in fair agreement with previous studies which demonstrated the better performance of iron-doped cerium oxides for CO oxidation [43] or the positive effect of ceria-copper domains copresence for the oxidation of CO and ethylene [44]. For example, Piumetti et al. [38] showed the presence of synergies with a set of cerium-copper oxides (with different Cu/Ce values) in the oxidation ethylene and CO. The best overall performance of both oxidation
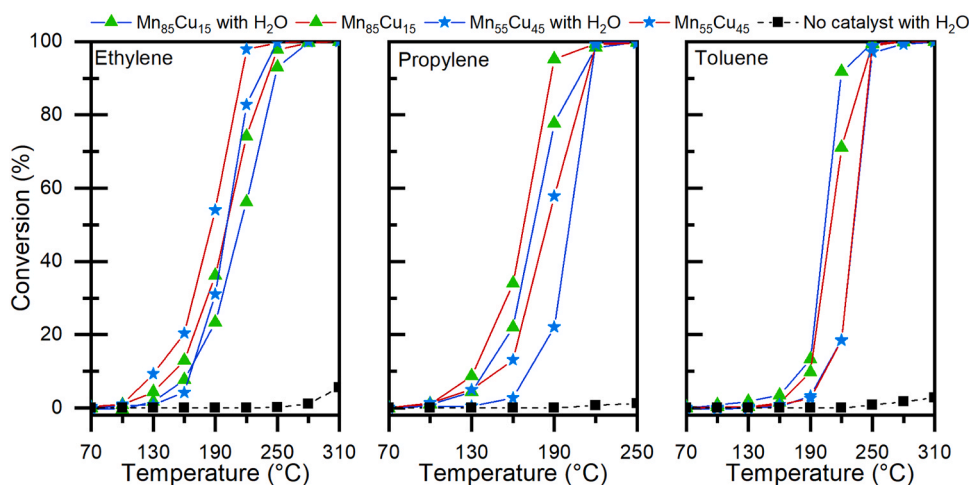
**Fig. 12.** Catalytic oxidation of ethylene (500 ppm), propylene (500 ppm), and toluene (500 ppm) in presence of 5 vol% content of water in the inlet gas stream: 10 vol% $O_2$, and $N_2$ to balance, W/F= 0.044 g h $L^{-1}$.
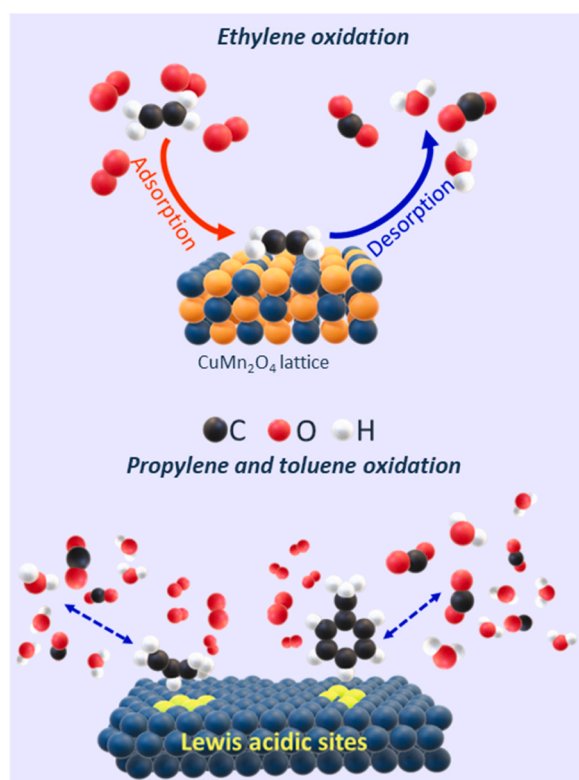


**Fig. 13.** Qualitative schematization of the catalytic oxidation mechanisms of ethylene, propylene and toluene.

reactions was attributed to the presence of $CeO_x$ and $CuO_x$ domains that cooperate synergistically, thereby leading to higher activity because of the easier surface reducibility and more abundant structural defects [45, 46]. As reported in Table 6, $Mn_{55}Cu_{45}$ is the most active catalyst at 130 °C (r = 5.9 $\mu mol \, h^{-1} \, m^{-2}$), although $Mn_{70}Cu_{30}$ performs better at higher temperature (namely, in the diffusive control). This can be likely due to the predominant presence of the crystalline phase $CuMn_2O_4$, the same as the best catalyst, together with a morphology more accessible to pollutant molecules than $Mn_{55}Cu_{45}$, (vide supra from $N_2$ physisorption at −196 °C and HR-TEM images). The more accessible 3-D structural topology can ease the diffusion of the oxidation products and consequently the ethylene conversion at higher temperature. On the other

hand, for the catalytic abatement of both propylene and toluene, the most effective catalyst is $Mn_{85}Cu_{15}$ both in the chemical kinetic region and at higher temperatures. Table 6 reports the specific oxidation rates for the three examined VOCs, calculated by adopting Eq. (3) (vide supra).

A possible explanation for the different efficiencies of these catalysts for the oxidation of the VOCs examined seems to be related to a different oxidation mechanism of toluene and propylene with respect to ethylene. In fact, the presence of acidic sites is an important factor favoring the catalytic oxidation of propylene [47,48], as well as the abatement of toluene [49,50]. In fact, there is a positive correlation between the propylene and toluene specific oxidation rate and the ammonia desorbed from Lewis acidic sites. $Mn_{85}Cu_{15}$, which gives the best results in the catalytic oxidation of propylene and toluene, presents two intense and distinct peaks in the $NH_3$ desorption profiles, indicating the presence of acidic sites and the highest amount of $NH_3$ desorbed in the range 250–410 °C. Ethylene oxidation seems to be mostly enhanced by the oxygen mobility, favored by the presence of oxygen defects such as oxygen vacancies, and redox ability ($Mn^{4+}/Mn^{3+}$, $Cu^+$ (%)). In fact, $Mn_{55}Cu_{45}$, the most active catalyst in the kinetic region, is the material with the greatest amount of oxygen desorbed, and it has the highest value of $O_\alpha/O_\beta$ ratio, $O_{def}$ (%), $Mn^{4+}/Mn^{3+}$ ratio, and relative abundance of $Cu^+$ (%) according to $O_2$-TPD and XPS analysis. The correlations between the ethylene oxidation rate and $O_\alpha/O_\beta$, $Mn^{4+}/Mn^{3+}$, and $Cu^+$ (%) are reported in Fig. 9. Moreover, theoretical studies have demonstrated that {110} crystal planes, present in this sample, promote the formation of oxygen vacancies [20] and enhance the catalytic oxidation of ethylene, in particular they are effective in the C-C and C-H bonds cleavage [51,52].

In order to analyze the catalytic stability of the most performing samples ($Mn_{85}Cu_{15}$ and $Mn_{55}Cu_{45}$), further catalytic tests were carried out on these oxides. Fig. 10 displays the catalytic conversion of each VOC as a function of temperature with three consecutive runs. As a whole, $Mn_{55}Cu_{45}$ shows an initial reduction in the catalytic performance for the oxidation of ethylene, possibly due to the reduction of $Cu^{2+}$ to $Cu^0$, according to the $H_2$-TPR outcomes, that occurs during the first run. Conversely, no meaningful deactivation was observed for the catalytic oxidation of propylene and toluene.

The VOC abatement as a function of time-on-stream (TOS) is shown in Fig. 11. The conversion of ethylene in the presence of $Mn_{55}Cu_{45}$ at 220 °C slightly decreased after the three cycles ($\Delta_{conv.}$ ~ 5 % over 7 h). The conversion of propylene in the presence of $Mn_{85}Cu_{15}$ at 190 °C is subjected to a slightly greater decrease than the ethylene conversion in the presence of $Mn_{55}Cu_{45}$ after the complete test ($\Delta_{conv.}$ ~ 10 % over 7 h). Toluene conversion at 250 °C is approximately 95 % for all the last

three cycles, and the first cycle has a lower conversion due to adsorption-desorption mechanisms. At 190 °C, the conversion of ethylene is approximately 40 % at the end of each cycle because of a progressive decrease. It is supposed that this behavior could be due to the gradual saturation of the catalyst's active sites until a dynamic equilibrium is achieved. The conversion of propylene at 160 °C, as well as toluene at 220 °C, is more stable than the conversion of ethylene at 190 °C. This fact can be interpreted as a further confirmation of the different oxidation mechanisms of propylene and toluene with respect to ethylene.

Fig. S2 shows the VOCs conversion as a function of time-on-stream (TOS) at a fixed temperature. The VOCs catalytic oxidation present a good stability during the 9 h of test, the outcomes confirm the results of the conversion in the time-on-stream configuration under alternating temperatures tests.

Fig. 12 displays the outcomes of the catalytic tests in dry and wet conditions. Both $Mn_{85}Cu_{15}$ and $Mn_{55}Cu_{45}$ were tested for the catalytic oxidation of ethylene, propylene, and toluene. As expected, the best performances for the oxidation of ethylene were achieved under dry conditions. In fact, considering the same temperature in the chemical kinetic region, there is a competitive adsorption of water versus ethylene molecules on the active sites that inhibits the whole activity [53]. In contrast, a weaker inhibition is observed for the oxidation of propylene and toluene in presence of $Mn_{85}Cu_{15}$. A similar behavior for propylene oxidation in analogous conditions was previously reported by Marin Figueredo et al. who, below 200 °C, observed a slight inhibition by the presence of water [54]. These findings can be a further indication of the different catalytic oxidation mechanism of propylene and toluene with respect to ethylene.

## 4. Conclusion

The aim of the present research was to examine a set of Cu-Mn oxide employed as catalysts for the total oxidation of three different representative VOCs (ethylene, propylene, and toluene). The samples were prepared through the SCS route, an efficient and simple synthesis method. All the oxides prepared result effective to achieve the total oxidation of the VOCs examined. The results of this investigation show that propylene and toluene are totally oxidized at 190 °C and 250 °C respectively in the presence of $Mn_{85}Cu_{15}$, while the total oxidation of ethylene is achieved at 190 °C in presence of $Mn_{55}Cu_{45}$. The catalytic test outcomes suggest that ethylene, propylene, and toluene follow different oxidation mechanisms, schematized in Fig. 13. Propylene and toluene oxidations are mainly favored by the presence of acidic sites, while ethylene oxidation seems to be mostly influenced by oxygen mobility and redox ability ($Mn^{4+}/Mn^{3+}$ ratio and $Cu^+$ species). Further analyses carried out on the most performing catalysts ($Mn_{85}Cu_{15}$ and $Mn_{55}Cu_{45}$) revealed good catalytic stability and low deactivation due to the presence of water vapor in the gas stream. These outcomes show that Cu-Mn oxides with the proper composition are suitable catalysts for VOC oxidation that could be further studied for their exploitation in stationary implants. Further research might explore different synthesis techniques to obtain catalysts with the same composition but an optimized morphology that will improve the catalytic activity of these metal oxides.

## CRediT authorship contribution statement

Conceptualization: **M.P., C.C.**; Methodology: **M.P., S.B., N.R., C.N.**; Investigation: **C.C., E.S.**; Funding acquisition: **N.R., D.F., F.G.**; Resources: **M.P., S.B., N.R., D.F., C.N., F.G.**; Writing and editing: **C.C., M. P., E.S.**; Supervision: **M.P.**

## Declaration of Competing Interest

The authors declare that they have no known competing financial

interests or personal relationships that could have appeared to influence the work reported in this paper.

## Appendix A. Supporting information

Supplementary data associated with this article can be found in the online version at doi:10.1016/j.cattod.2023.114292.

## References

[1] M. Piumetti, D. Fino, N. Russo, Mesoporous manganese oxides prepared by solution combustion synthesis as catalysts for the total oxidation of VOCs, Appl. Catal. B Environ. 163 (2015) 277–287, https://doi.org/10.1016/j.apcatb.2014.08.012.

[2] M.J. Marin Figueredo, T. Andana, S. Bensaid, M. Dosa, D. Fino, N. Russo, M. Piumetti, Cerium–copper–manganese oxides synthesized via solution combustion synthesis (SCS) for total oxidation of VOCs, Catal. Lett. 150 (2020) 1821–1840, https://doi.org/10.1007/s10562-019-03094-x.

[3] S.H. Taylor, Preface: catalytic aspects of complete oxidation of volatile organic compounds, Top. Catal. 52 (2009) 457, https://doi.org/10.1007/s11244-009-9179-3.

[4] W.B. Li, J.X. Wang, H. Gong, Catalytic combustion of VOCs on non-noble metal catalysts, Catal. Today 148 (2010) 81–87, https://doi.org/10.1016/j.cattod.2009.03.007.

[5] M.S. Kamal, S.A. Razzak, M.M. Hossain, Catalytic oxidation of volatile organic compounds (VOCs) - a review, Atmos. Environ. 140 (2016) 117–134, https://doi.org/10.1016/j.atmosenv.2016.05.031.

[6] F. Sapio, F. Millo, D. Fino, A. Monteverde, E. Sartoretti, A. Bianco, L. Postrioti, A. Tarabocchia, G. Buitoni, G. Brizi, Experimental and numerical analysis of latest generation diesel aftertreatment systems, SAE Tech. Pap. (2019) 2019–Septe, https://doi.org/10.4271/2019-24-0142.

[7] L.F. Liotta, Catalytic oxidation of volatile organic compounds on supported noble metals, Appl. Catal. B Environ. 100 (2010) 403–412, https://doi.org/10.1016/j.apcatb.2010.08.023.

[8] L. Yosefi, M. Haghighi, S. Allahyari, R. Shokrani, S. Ashkriz, Abatement of toluene from polluted air over Mn/Clinoptilolite-CeO<sub>2 nanopowder: impregnation vs. ultrasound assisted synthesis with various Mn-loading, Adv. Powder Technol. 26 (2015) 602–611, https://doi.org/10.1016/j.apt.2015.01.009.

[9] M. Piumetti, F.S. Freyria, M. Armandi, F. Geobaldo, E. Garrone, B. Bonelli, Fe- and V-doped mesoporous titania prepared by direct synthesis: characterization and role in the oxidation of AO7 by H2O2 in the dark, Catal. Today 227 (2014) 71–79, https://doi.org/10.1016/j.cattod.2013.11.013.

[10] Le. Minh Cam Nguyen Thi Mo, Stability of Cu-doped manganese oxide catalyst in the oxidation of m-Xylene, Russ. J. Phys. Chem. A 93 (2019) 2016–2022, https://doi.org/10.1134/S0036024419100182.

[11] Y. Gao, Z. Wang, C. Cui, B. Wang, W. Liu, W. Liu, L. Wang, Amorphous manganese oxide as highly active catalyst for soot oxidation, Environ. Sci. Pollut. Res. 27 (2020) 13488–13500, https://doi.org/10.1007/s11356-020-07909-y.

[12] E. Sartoretti, C. Novara, M. Fontana, F. Giorgis, M. Piumetti, S. Bensaid, N. Russo, D. Fino, New insights on the defect sites evolution during CO oxidation over doped ceria nanocatalysts probed by in situ Raman spectroscopy, Appl. Catal. A Gen. 596 (2020), 117517, https://doi.org/10.1016/j.apcata.2020.117517.

[13] V.H. Vu, J. Belkouch, A. Ould-Dris, B. Taouk, Removal of hazardous chlorinated VOCs over Mn-Cu mixed oxide based catalyst, J. Hazard. Mater. 169 (2009) 758–765, https://doi.org/10.1016/j.jhazmat.2009.04.010.

[14] F.A. Deorsola, S. Andreoli, M. Armandi, B. Bonelli, R. Pirone, Unsupported nanostructured Mn oxides obtained by solution combustion synthesis: textural and surface properties, and catalytic performance in NOx SCR at low temperature, Appl. Catal. A Gen. 522 (2016) 120–129, https://doi.org/10.1016/j.apcata.2016.05.002.

[15] B. Puértolas, A. Smith, I. Vázquez, A. Dejoz, A. Moragues, T. Garcia, B. Solsona, The different catalytic behaviour in the propane total oxidation of cobalt and manganese oxides prepared by a wet combustion procedure, Chem. Eng. J. 229 (2013) 547–558, https://doi.org/10.1016/j.cej.2013.06.041.

[16] J. Hu, W.B. Li, R.F. Liu, Highly efficient copper-doped manganese oxide nanorod catalysts derived from CuMnO hierarchical nanowire for catalytic combustion of

VOCs, Catal. Today 314 (2018) 147–153, https://doi.org/10.1016/j.cattod.2018.02.009.

[17] T.J. Clarke, S.A. Kondrat, S.H. Taylor, Total oxidation of naphthalene using copper manganese oxide catalysts, Catal. Today 258 (2015) 610–615, https://doi.org/10.1016/j.cattod.2015.01.032.

[18] K.K. Hazarika, H. Talukdar, P. Sudarsanam, S.K. Bhargava, P. Bharali, Highly dispersed Mn2O3−Co3O4 nanostructures on carbon matrix as heterogeneous Fenton-like catalyst, Appl. Organomet. Chem. 34 (2020) 1–13, https://doi.org/10.1002/aoc.5512.

[19] M. Dosa, M. Piumetti, S. Bensaid, T. Andana, C. Novara, F. Giorgis, D. Fino, N. Russo, Novel Mn–Cu-containing CeO2 nanopolyhedra for the oxidation of CO and diesel soot: effect of dopants on the nanostructure and catalytic activity, Catal. Lett. 148 (2018) 298–311, https://doi.org/10.1007/s10562-017-2226-y.

[20] W.J. Xue, Y.F. Wang, P. Li, Z.T. Liu, Z.P. Hao, C.Y. Ma, Morphology effects of Co3O4 on the catalytic activity of Au/Co3O4 catalysts for complete oxidation of trace ethylene, Catal. Commun. 12 (2011) 1265–1268, https://doi.org/10.1016/j.catcom.2011.04.003.

[21] A. Ashok, A. Kumar, R.R. Bhosale, F. Almomani, S.S. Malik, S. Suslov, F. Tarlochan, Combustion synthesis of bifunctional LaMO3 (M = Cr, Mn, Fe, Co, Ni) perovskites for oxygen reduction and oxygen evolution reaction in alkaline media, J. Electroanal. Chem. 809 (2018) 22–30, https://doi.org/10.1016/j.jelechem.2017.12.043.

[22] M.B. Ward, R. Brydson, A.P. Brown, R.F. Cochrane, Analysis of strain in manganese nanoparticles using the optical moiré technique, J. Phys. Conf. Ser., 126 (2008). https://doi.org/10.1088/1742–6596/126/1/012068.

[23] J.E. Post, D.A. McKeown, P.J. Heaney, Raman spectroscopy study of manganese oxides: tunnel structures, Am. Miner. 105 (2020) 1175–1190, https://doi.org/10.2138/am-2020-7390.

[24] F. Buciuman, F. Patcas, R. Craciun, D.R.T. Zahn, Vibrational spectroscopy of bulk and supported manganese oxides, Phys. Chem. Chem. Phys. 1 (1999) 185–190, https://doi.org/10.1039/a807821a.

[25] J. Wang, J. Chen, L. Peng, H. Zhang, Z. Jiang, K. Xiong, Q. Yang, J. Chen, N. Yang, On the CuO-Mn2O3 oxide-pair in CuMnOx multi-oxide complexes: structural and catalytic studies, Appl. Surf. Sci. 575 (2022), https://doi.org/10.1016/j.apsusc.2021.151733.

[26] M. Verma, V. Kumar, A. Katoch, Sputtering based synthesis of CuO nanoparticles and their structural, thermal and optical studies, Mater. Sci. Semicond. Process. 76 (2018) 55–60, https://doi.org/10.1016/j.mssp.2017.12.018.

[27] G. Avgouropoulos, T. Ioannides, Selective CO oxidation over CuO-CeO2 catalysts prepared via the urea-nitrate combustion method, Appl. Catal. A Gen. 244 (2003) 155–167, https://doi.org/10.1016/S0926-860X(02)00558-6.

[28] M.J.M. Figueredo, C. Cocuzza, S. Bensaid, D. Fino, M. Piumetti, N. Russo, Catalytic abatement of volatile organic compounds and soot over manganese oxide catalysts, Materials 14 (2021) 4534, https://doi.org/10.3390/ma14164534.

[29] Y. Zhang, Z. Zeng, Y. Li, Y. Hou, J. Hu, Z. Huang, Effect of the A-site cation over spinel AMn2O4 (A = Cu2+, Ni2+, Zn2+) for toluene combustion: enhancement of the synergy and the oxygen activation ability, Fuel 288 (2021), https://doi.org/10.1016/j.fuel.2020.119700.

[30] L.F. Liotta, M. Ousmane, G. Di Carlo, G. Pantaleo, G. Deganello, G. Marcì, L. Retailleau, A. Giroir-Fendler, Total oxidation of propene at low temperature over Co3O4-CeO2 mixed oxides: role of surface oxygen vacancies and bulk oxygen mobility in the catalytic activity, Appl. Catal. A Gen. 347 (2008) 81–88, https://doi.org/10.1016/j.apcata.2008.05.038.

[31] D.W. Kwon, K.B. Nam, S.C. Hong, Influence of tungsten on the activity of a Mn/Ce/W/Ti catalyst for the selective catalytic reduction of NO with NH3 at low temperatures, Appl. Catal. A Gen. 497 (2015) 160–166, https://doi.org/10.1016/j.apcata.2015.01.013.

[32] D. Fang, F. He, D. Li, J. Xie, First principles and experimental study of NH 3 adsorptions on MnO x surface, Appl. Surf. Sci. 285 (2013) 215–219, https://doi.org/10.1016/j.apsusc.2013.08.039.

[33] T. Andana, M. Piumetti, S. Bensaid, N. Russo, D. Fino, R. Pirone, CO and soot oxidation over Ce-Zr-Pr oxide catalysts, Nanoscale Res. Lett. 11 (2016), https://doi.org/10.1186/s11671-016-1494-6.

[34] M. Wang, E.D. Park, J.M. Kim, J.E. Yie, Manganese oxide catalysts for NOx reduction with NH3 at low temperatures, Appl. Catal. A Gen. 327 (2007) 261–269, https://doi.org/10.1016/j.apcata.2007.05.024.

[35] I.S. Zhidkov, A.I. Kukharenko, R.N. Maksimov, L.D. Finkelstein, S.O. Cholakh, V.V. Osipov, E.Z. Kurmaev, Optical transparency and local electronic structure of Yb-doped Y 2 O 3 ceramics with tetravalent additives, Symmetry 11 (2019) 1–8, https://doi.org/10.3390/sym11020243.

[36] Y. Hu, Z. Li, W. Pan, Sandwich-like transparent ceramic demonstrates ultraviolet and visible broadband downconversion luminescence, RSC Adv. 8 (2018) 13200–13204, https://doi.org/10.1039/c8ra02195c.

[37] S.A. Abdullah, M.Z. Sahdan, N. Nayan, Z. Embong, C.R.C. Hak, F. Adriyanto, Neutron beam interaction with rutile TiO2 single crystal (1 1 1): Raman and XPS study on Ti3+-oxygen vacancy formation, Mater. Lett 263 (2020), 127143, https://doi.org/10.1016/j.matlet.2019.127143.

[38] M. Piumetti, S. Bensaid, T. Andana, N. Russo, R. Pirone, D. Fino, Cerium-copper oxides prepared by solution combustion synthesis for total oxidation reactions: from powder catalysts to structured reactors, Appl. Catal. B Environ. 205 (2017) 455–468, https://doi.org/10.1016/j.apcatb.2016.12.054.

[39] A. Elmhamdi, L. Pascual, K. Nahdi, A. Martínez-Arias, Structure/redox/activity relationships in CeO2/CuMn2O4 CO-PROX catalysts, Appl. Catal. B Environ. 217 (2017) 1–11, https://doi.org/10.1016/j.apcatb.2017.05.070.

[40] S.C. Kim, W.G. Shim, Catalytic combustion of VOCs over a series of manganese oxide catalysts, Appl. Catal. B Environ. 98 (2010) 180–185, https://doi.org/10.1016/j.apcatb.2010.05.027.

[41] S. Hassan, R. Kumar, A. Tiwari, W. Song, L. van Haandel, J.K. Pandey, E. Hensen, B. Chowdhury, Role of oxygen vacancy in cobalt doped ceria catalyst for styrene epoxidation using molecular oxygen, Mol. Catal. 451 (2018) 238–246, https://doi.org/10.1016/j.mcat.2018.01.025.

[42] M. Shaw, D. Samanta, S. Bera, M.K. Mahto, M.A. Salam Shaik, S. Konar, I. Mondal, D. Dhara, A. Pathak, Role of surface oxygen vacancies and oxygen species on CuO nanostructured surfaces in model catalytic oxidation and reductions: insight into the structure-activity relationship toward the performance, Inorg. Chem. 61 (2022) 14568–14581, https://doi.org/10.1021/acs.inorgchem.2c01467.

[43] T.R. Sahoo, M. Armandi, R. Arletti, M. Piumetti, S. Bensaid, M. Manzoli, S.R. Panda, B. Bonelli, Pure and Fe-doped CeO2 nanoparticles obtained by microwave assisted combustion synthesis: physico-chemical properties ruling their catalytic activity towards CO oxidation and soot combustion, Appl. Catal. B Environ. 211 (2017) 31–45, https://doi.org/10.1016/j.apcatb.2017.04.032.

[44] M. Dosa, M.J. Marin-figueredo, E. Sartoretti, C. Novara, F. Giorgis, S. Bensaid, D. Fino, N. Russo, M. Piumetti, Cerium-copper oxides synthesized in a multi-inlet vortex reactor as effective nano for CO and Ethene Oxidation Reactions, Catalysts 12 (2022), https://doi.org/10.3390/catal12040364.

[45] M. Piumetti, Molecular Dynamics and Complexity in Catalysis and Biocatalysis, 2022. doi: 10.1007/978-3-030-88500-7.

[46] M. Piumetti, N. Lygeros, Complexity in catalysis, Mol. Dyn. Complex. Catal. Biocatal. (2022) 113–144, https://doi.org/10.1007/978-3-030-88500-7_5.

[47] R. Sakai, K. Ueda, J. Ohyama, A. Oda, K. Deguchi, S. Ohki, A. Satsuma, Preferential oxidation of propene in gasoline exhaust conditions over supported vanadia catalysts, J. Catal. 408 (2022) 261–269, https://doi.org/10.1016/j.jcat.2022.03.012.

[48] E. Janiszewska, A. Held, K. Nowińska, S. Kowalak, One-pot synthesis of vanadium-containing silica SBA-3 materials and their catalytic activity for propene oxidation, RSC Adv. 9 (2019) 4671–4681, https://doi.org/10.1039/c8ra10171j.

[49] S.A.C. Carabineiro, X. Chen, M. Konsolakis, A.C. Psarras, P.B. Tavares, J.J.M. Órfão, M.F.R. Pereira, J.L. Figueiredo, Catalytic oxidation of toluene on Ce-Co and La-Co mixed oxides synthesized by exotemplating and evaporation methods, Catal. Today 244 (2015) 161–171, https://doi.org/10.1016/j.cattod.2014.06.018.

[50] Q.F. Deng, T.Z. Ren, Z.Y. Yuan, Mesoporous manganese oxide nanoparticles for the catalytic total oxidation of toluene, React. Kinet. Mech. Catal. 108 (2013) 507–518, https://doi.org/10.1007/s11144-012-0528-z.

[51] R.J. Isaifan, S. Ntais, E.A. Baranova, Particle size effect on catalytic activity of carbon-supported Pt nanoparticles for complete ethylene oxidation, Appl. Catal. A Gen. 464–465 (2013) 87–94, https://doi.org/10.1016/j.apcata.2013.05.027.

[52] Y. Gao, X. Huo, T. Li, R. Jiang, Q. Zhu, H. Ren, Mechanisms and energetics of complete ethylene oxidation on a PdAu bimetallic catalyst from a theoretical perspective, J. Phys. Chem. C (2022), https://doi.org/10.1021/acs.jpcc.2c01277.

[53] J. Li, R. Wang, J. Hao, Role of lattice oxygen and lewis acid on ethanol oxidation over OMS-2 catalyst, J. Phys. Chem. C 114 (2010) 10544–10550, https://doi.org/10.1021/jp102779u.

[54] M.J. Marin Figueredo, M. Piumetti, D. Fino, N. Russo, C. Cocuzza, S. Bensaid, Catalytic oxidation of soot and volatile organic compounds over Cu and Fe doped manganese oxides prepared via sol-gel synthesis, SAE Tech. Pap. (2021), https://doi.org/10.4271/2021-24-0088.